Final Draft
of the original manuscript:

Manente Andre, N.; Goushegir, S.M.; Scharnagl, N.; dos Santos, J.F.;
Canto, L.B., Amancio-Filho, S.T.:

Composite surface pre-treatments: improvement on adhesion mechanisms and mechanical performance of metal-composite friction spot joints with additional film interlayer

In: The Journal of Adhesion (2018) Taylor & Francis

DOI: 10.1080/00218464.2017.1378101

“Composite surface pre-treatments: Improvement on bonding mechanisms and mechanical performance of metal-composite friction spot joints with additional film interlayer”

Natália Manente André[a,b], Seyed M. Goushegir[b], Nico Scharnagl[c], Jorge F. dos Santos[b], Leonardo B. Canto[a], and Sergio T. Amancio-Filho[b,d*]

[a] Postgraduate Program in Materials Science and Engineering, Federal University of Sao Carlos (UFSCar), São Carlos, Brazil

[b] Helmholtz-Zentrum Geesthacht, Centre for Materials and Coastal Research, Institute of Materials Research, Materials Mechanics, Solid State Joining Processes, Geesthacht, Germany

[c] Helmholtz-Zentrum Geesthacht, Centre for Materials and Coastal Research, Institute of Materials Research, Magnesium Innovation Center (MagIC), Corrosion and Surface Technology, Geesthacht, Germany

[d] Hamburg University of Technology, Institute of Polymer Composites, Hamburg, Germany

*Corresponding author: Tel./Fax: +49 4152 87 2066 / 2033 email: sergio.amancio@hzg.de

Abstract

Friction spot joints of aluminum alloy 2024-T3 and carbon-fiber-reinforced polyphenylene sulfide were produced with PPS film interlayer. Mechanical grinding, sandblasting and sandblasting combined with plasma activation were performed on the composite part to enhance the interface adhesion. The aluminum part was sandblasted in all cases. The surface features – roughness, wettability and chemical activation – were correlated with the ultimate lap shear force of the joints. The composite surface with the highest surface roughness (sandblasting: 5.3 ± 0.6 µm) led to a joint approximately 95% stronger (3068 ±192 N) than the joint with the lowest surface roughness (mechanical grinding: 0.6 ± 0.1 µm, 1573 ± 84 N). The increase in surface roughness generated crevices and enlarged the effective contact surface area. This led to a better micro-mechanical interlocking between the PPS film, melted during the joining process, and the composite surface. Although functional groups were identified in the plasma treated specimens using X-ray photoelectron spectroscopy, the plasma activation did not contribute to the mechanical strength of the joints. It is believed that the plasma activation was lost due to the high temperature achieved during the joining process and the resultant melting of the PPS. The fracture surface analysis of the joints supported the conclusion that sandblasting was the most effective treatment, maximizing the mechanical performance of the joints. Impressions containing pieces of carbon fibers were identified on the interlayer

surface after mechanical testing. It indicates effective micro-mechanical interlocking at the interface of interlayer-composite achieved with the sandblasted specimens.

Keywords: Friction Spot Joining, surface treatment, adhesion, composite, mechanical performance

1. Introduction

In the pursuit of the reduction in fuel consumption and CO_2 emission, the use of metal-polymer composite hybrid structures has turned into a lightweight attractive solution for the transport industry [1–3]. However, the feasibility of joining such dissimilar materials is still a query due to the contrast in the physicochemical properties of those classes of materials. A wide variety of joining technologies has been investigated for metal-composite structures. Among them, one can find traditional techniques – e.g. mechanical fastening [4] and adhesive bonding [5] – and recently developed technologies, such as resistance [6], ultrasonic [7], laser [8] and induction welding [9]. Amongst joining techniques recently developed for hybrid structures, the present work highlights a recently introduced friction-based process, the Friction Spot Joining.

Friction Spot Joining (FSpJ) is an alternative friction-based joining technique for hybrid structures developed at Helmholtz-Zentrum Geesthacht (HZG), Germany [10]. The FSpJ is a suitable process for joining metal-polymer or composite hybrid structures. By using optimized process parameters, polymer degradation and damage to the fibers network of the composite - which cause a decrease in the mechanical performance of the hybrid joint – may be avoided or reduced. Additionally, FSpJ presents short joining cycles, from 2 to maximum 8 seconds [11].

The feasibility of the FSpJ process was investigated for different combinations of materials such as magnesium alloy AZ31 [11], AA6181-T4 [12], and AA2024-T3 [13] to carbon fiber (CF-) and glass fiber (GF-) reinforced polymers (RP). Additionally, in a recent study [14] we showed that the use of a polymer film interlayer between metal and composite parts improves the mechanical performance of FSp joints by enhancing bonding mechanisms. The use of a film interlayer was encouraged based on the advantages offered by the weld-bonding technology, which suggests the combination of welding and adhesive bonding to improve joints mechanical performance [15]. During the FSpJ process, the semi-crystalline interlayer is melted and recrystallized, forming a thin layer of reconsolidated polymer in between the joining parts. As a result, the joints presented larger bonding area and pronounced adhesion forces provided by the film interlayer [14]. Therefore, superior load distribution as well as static and

fatigue performance are achieved [14,16]. The joints with film showed static strength 55% higher along with a fatigue life four times longer than the respective joints without film [16]. Further advantages such as exemption of curing time, compared to the currently used industrial adhesives [17], can be mentioned.

Surface modification has been extensively explored to enhance adhesion strength and durability in adhesively bonded joints [17,18]. Promoting adhesion in composite materials is, however, a challenging issue. Composites often present a very smooth surface full of contaminants (such as release and bagging agents) owing to the molding process. Furthermore, most polymers possess low surface energy which makes the interaction with the adhesive difficult [19]. Therefore, suitable surface treatments are required to change the surface state (such as surface energy and morphology) and bonding behavior of the composites.

Mechanical surface treatments are simple and effective techniques to modify the surface by altering morphology and roughness. A rough surface allows the adhesive to flow in and around the generated irregularities, promoting an effective mechanical interlocking with the substrate [17]. Changes in surface energy may also occur due to the removal of material, creating sites on the substrate for chemical bonds with the adhesive [19]. Encinas *et al.* [20] tailored the wettability of high-density polyethylene (HDPE), low-density polyethylene (LDPE), polypropylene (PP) and silicone through mechanical abrasion. They demonstrated a decrease in the contact angle as the surface roughness was increased. Wingfield *et al.* [19] studied alumina grit-blasting and SiC abrasion of carbon-fiber-reinforced polyether ether ketone (CF-PEEK), CF-epoxy and GF-PP for single-lap bonded joints. The authors reported extensive improvement in the bond strength of the pre-treated joints (35 MPa) compared to those produced with as-received polymer sheets (8 MPa).

Energetic surface treatments, such as plasma activation, are other types of treatments, which enhance the adhesion mainly due to the increase of surface energy. The plasma oxidizes the polymer surface, leading to the removal of organic contaminants and introduction of polar functional groups. Thus, more reactive and wettable surfaces can be created [21]. Surfaces in contact with the plasma are bombarded by high energetic species. During the collisions, the energy of the species is transferred from the plasma to the solid surface and dissipated through several physical and chemical processes, resulting in a higher energetic modified surface. These superficial changes can achieve depths from several hundred angstroms to 10 μm without changing any bulk properties of the material [22]. Kim *et al.* [23]

demonstrated the effect of plasma treatment on the adhesive bonding of a carbon/epoxy composite. The authors showed a decrease in contact angle while the surface energy increased, indicating a more effective wetting of the surface and better adhesion between composite and adhesive. Iqbal *et al.* [24] investigated the surface modification of high-performance polymers, such as CF- and GF-PPS and PEEK, by plasma treatment and its influence on the adhesive bonding of these materials. It was demonstrated that the strength of adhesively bonded joints improved from 6 to 22 MPa due to the formation of functional groups after plasma activation.

In the sense of further improving the adhesion between the film interlayer and joining parts in the metal-composite friction spot joints, the present study investigated three different surface pre-treatments for the composite part of the joints. The influence of metal surface pre-treatments on the mechanical performance of FSp joints was addressed by Goushegir *et al.* [13] and Esteves *et al.* [25]. In both works, it was demonstrated that the joint's lap shear strength could be increased up to 160% when a suitable surface pre-treatment was applied on the metallic surface in comparison to the as-received condition. In this work, mechanical grinding, sandblasting and plasma activation of the composite part were investigated in the AA2024-T3/PPS/CF-PPS hybrid joints. Different surface features such as roughness and wettability were evaluated using scanning laser and electron microscopy as well as contact angle measurements. X-ray photoelectron spectroscopy (XPS) was also used to investigate the chemical changes of the surface prior to the joining process. Such features were then correlated with the bonding mechanisms and the lap shear static strength of the joints, along with a brief analysis of the joints failure mechanisms.

2. Friction Spot Joining (FSpJ)

Friction Spot Joining (FSpJ) is a prize-winning joining process for metal-polymer or composite hybrid structures [26,27]. The technique employs a non-consumable tool comprised of three pieces: a pin, a sleeve and a clamping ring [11]. The pin and sleeve move axially and rotate independently of each other, whereas the clamping ring is stationary. Prior to the joining process, the parts are clamped between a backing plate and the clamping ring to ensure intimate contact between them during the process. Moreover, clamping is responsible for avoiding separation of the joining parts during the cooling stage at the end of the joining process.

At the first step of the process, the rotating sleeve plunges into the upper sheet (a metal sheet in this work, Figure 1-1). The friction between the sleeve and the metal part locally increases the temperature to below the melting point of the metal [12,13]. Therefore, a certain volume of the metal around the tool is softened and plastically deformed. The pin is simultaneously retracted, forming a keyhole (acting as a reservoir) where the softened metal flows into (Figure 1-1). At the second step, sleeve and pin are both driven back to the original position (metal surface). In this movement, the pin pushes back the entrapped softened metal into the metal part, refilling the keyhole formed during the sleeve plunging motion (Figure 1-2). Finally, the tool is retracted from the metal surface and the spot joint consolidates under pressure (Figure 1-3). Note that the sleeve plunges shallowly into the metal piece without reaching the interface, avoiding any damage to the fiber network of the composite and degradation of the polymer matrix. Four main FSpJ process parameters can be identified: rotational speed (RS), plunge depth (PD), joining time (JT), and joining pressure (JP) [28].

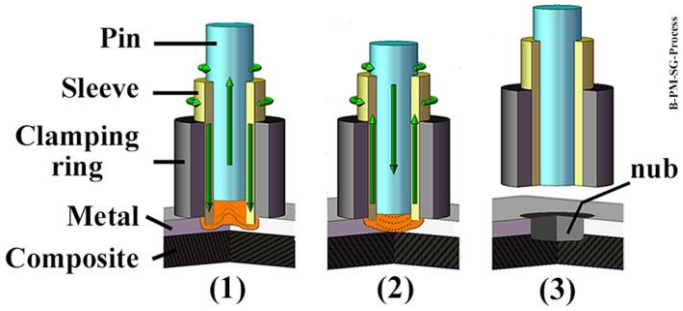

Figure 1: Schematic description of the FSpJ technique. (1) The sleeve plunging softens the metal alloy; (2) spot refilling; (3) joint consolidation. (Authorized reproduction from [13])

In friction spot metal-composite joints there are two main bonding mechanisms responsible for the joints strength: mechanical interlocking and adhesion forces [11,13]. As previously discussed, during the joining process the softened metal is plastically deformed by the tool plunging movement. The metal deformation creates a geometrical undercut known as “metallic nub” (Figure 2-A). The metallic nub provides macro-mechanical interlocking between the joining parts, supporting the joint strength under shear loading. Moreover, micro-mechanical interlocking is established at the joint interface by the entrapment of the composite matrix and some of the fibers into the irregularities of the metal’s surface (Figure 2-B) [13]. In addition, frictional heat is conducted from the metal to the composite in the overlap area of the joint. The conducted heat melts/softens a thin layer of polymer at the metal-composite

interface. In the case of using the film interlayer, the frictional heat melts/softens the interlayer material as well. After the cooling stage, this polymeric layer reconsolidates and contributes to the adhesion forces at the metal-composite interface [13].

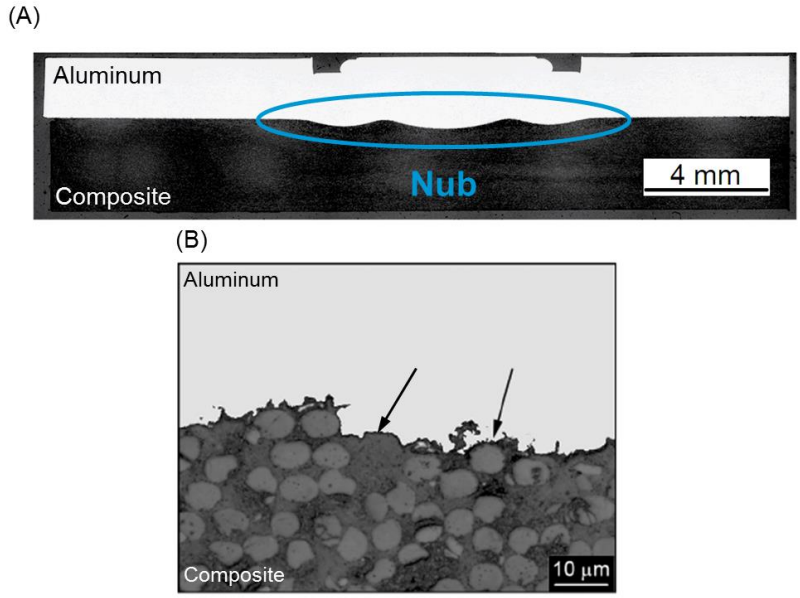

Figure 2: (A) A typical cross section of an FSp metal-polymer composite hybrid FSp joint; the ellipse indicates the metallic nub formed at the interface, and (B) detail of the metal-composite interface; the arrows indicate the micro-mechanical interlocking by polymer entrapment and fiber attachment into the aluminum irregularities. (Adapted from [13]).

3. Materials and Methods

3.1. Aluminum alloy 2024-T3

The aluminum alloy 2024-T3 in bare condition (rolled sheets, 2 mm thick) supplied by Costellium, France was used in this study. This is a precipitation hardenable alloy, which has Cu and Mg as the main alloying elements. This alloy is the predominant 2XXX series aircraft alloy due to the excellent specific strength and fatigue performance, conformability and surface finishing capabilities [29]. The chemical composition of the AA2024-T3 alloy obtained by chemical analysis is shown in Table 1. Table 2 lists the main physical and mechanical properties of the alloy used in this work.

Table 1: Chemical composition of AA2024-T3 used in this work.

Element	Cu	Mg	Mn	Fe	Zn	Si	Ti	Cr	Al
Wt%	4.55	1.49	0.45	0.17	0.16	0.10	0.02	≤ 0.01	Bal

Table 2: Selected physical and mechanical properties of AA2024-T3 [29].

Tensile Strength (TL direction) [MPa]	Yield Strength (TL direction) [MPa]	Elongation [%]	Incipient Melting Temperature [°C]	Thermal Conductivity [W m^{-1} K^{-1}]	Coefficient of Thermal Expansion , 20–300°C [µm m^{-1} $°C^{-1}$]
437	299	21	502	121	24.7

3.2. Carbon-fiber-reinforced polyphenylene sulfide (CF-PPS) and PPS film

The composite part used in this work was a carbon-fiber-reinforced polyphenylene sulfide (CF-PPS), 2.17 mm of nominal thickness, supplied by Tencate, Netherlands (CETEX®). The CF-PPS used in this study was a quasi-isotropic laminate with 43 wt% carbon fibers woven fabric in the five-harness satin configuration. The layers of PPS and 7 plies of carbon fiber fabric are overlapped in the [(0.90)/(±45)]3/(0.90) sequence. CF-PPS is a high-temperature, high-performance thermoplastic composite certified for multiple applications in the aerospace field, such as "J-Nose" subframe wings and engine pylon cover of Airbus A340-500/600 [30]. Table 3 lists the main physical and mechanical properties of the CF-PPS composite.

Table 3: Selected physical and mechanical properties of the CF-PPS at room temperature [30].

Tensile Strength (warp/weft) [MPa]	In-Plane Shear Strength [MPa]	Glass Transition Temperature [°C]	Melting Temperature [°C]	Thermal Conductivity [W m^{-1} K^{-1}]	Coefficient of Thermal Expansion, 23–300°C [µm m^{-1} $°C^{-1}$]
790/750	119	120	280	0.19	52.2

A 100 µm thick PPS film supplied by LITE P, Austria was employed as the interlayer between the aluminum alloy and composite. This is a thermoplastic film, with a low degree of crystallinity (7%) [31]. The main properties of the PPS film used in this work are listed in Table 4.

Table 4: Selected physical and mechanical properties the PPS film at room temperature [31].

Tensile Strength [MPa]	Glass Transition Temperature [°C]	Melting Temperature [°C]	Thermal Conductivity [W m^{-1} K^{-1}]	Coefficient of Thermal Expansion, 23–300°C [µm m^{-1} $°C^{-1}$]
85	92	280	0.24	52.0

3.3. Experimental Procedure

3.3.1. Surface Preparation

Surface pre-treatments on both aluminum and composite were carried out in order to enhance the adhesion between the joining parts. Aluminum and composite were cleaned followed by surface pre-treatments prior to the joining process. For the aluminum, only sandblasting was performed based on the successful past investigations [13]. In the case of the composite, three different pre-treatments were applied: mechanical grinding, sandblasting and plasma activation. Details of the performed surface pre-treatments are described next.

Aluminum

Sandblasting was carried out using a Normfinish® equipment (Holland). Corundum (Al_2O_3) with an average particles size of 100-150 µm was employed as the blasting medium. The distance between the samples and the pistol was fixed at 20 cm. The angle between the aluminum surface and the pistol was 45°. The sandblasting was applied for 10 seconds with a pressure of 0.6 MPa. The selected parameters for the treatment of the aluminum part were chosen in accordance with the previous investigation [13].

Composite

A set of composite samples was manually ground in 0°, 90° and ±45° directions to avoid any preferential groove orientation. Two different SiC papers were used to perform mechanical grinding on the composite surfaces: P320 (average particle size of 46 µm) and P1200 (average particle size of 15 µm).

Another set of composite samples was sandblasted. Two angles between the surface and the pistol were investigated: 90° and 45º. In the case of blasting angle of 90º, the blasting times were 5 and 10 s. In the case of blasting angle of 45°, the blasting time was 5 s to avoid excessive removal of the composite's matrix. A blasting manometric pressure of 0.3 MPa was applied to avoid extensive removal of the matrix and damage to the carbon fibers. The equipment, the blast medium and the distance between samples and the pistol were the same employed for aluminum samples.

The surface pre-treated specimens were then cleaned with compressed air followed by ethanol cleaning in an ultrasonic bath for 3 minutes. This was performed to remove debris and particles generated during both mechanical pre-treatments.

In order to investigate the influence of chemical activation on the mechanically treated surfaces, a set of sandblasted composite samples (sandblasted at 45°) was subsequently plasma-treated. Low-pressure

plasma pre-treatment was performed using a plasma generator equipment (Diener Electronic GmbH) with a power of 100 W and 0.5 mbar of chamber pressure. Oxygen was used as the chamber gas. Two different treatment times were tested: 5 and 10 minutes. In this case, a set of PPS films was also plasma-treated with the identical parameters used for the composite.

Table 5 summarizes the surface pre-treatments carried out on the joining parts.

Table 5: Summary of surface pre-treatments on the joining parts.

Material	Surface Pre-treatment	Symbol	Parameters
Aluminum	Sandblasting	S1	Al_2O_3, 100 – 150 µm, 20 cm distance, 45°, 10 s, 0.6 MPa
Composite	Sandblasting	S2	Al_2O_3, 100 – 150 µm, 20 cm distance, 90°, 5 s, 0.3 MPa
		S3	Al_2O_3, 100 – 150 µm, 20 cm distance, 90°, 10 s, 0.3 MPa
		S4	Al_2O_3, 100 – 150 µm, 20 cm distance, 45°, 5 s, 0.3 MPa
	Mechanical Grinding	M1	SiC P1200, 0°/90°/±45°
		M2	SiC P320, 0°/90°/±45°
	Sandblasting + Plasma Activation	S4 + P1	S4 + O_2, 100 W, 0.5 mbar, 5 min
		S4 + P2	S4 + O_2, 100 W, 0.5 mbar, 10 min

3.3.2. Surface Characterization

The surface of the specimens after pre-treatments and prior to the joining process was analyzed as described below.

Surface Topography

The surface roughness of the aluminum and composite was analyzed using the non-contact method with a Laser Scanning Confocal Microscope (Keyence, Japan). The surface roughness was

evaluated based on the EN ISO 25178-2 standard to correlate the mechanical performance of the joints with the surface topography of the specimens.

The arithmetic average surface roughness parameter (R_a) was calculated from three different areas on each surface. Five randomly treated samples were examined from each pre-treatment. The average of the 15 measured values was taken as the average surface roughness for each surface pre-treatment.

Additionally, the surface of the specimens was examined by Scanning Electron Microscopy (SEM) (FEI, QUANTA FEG 650). Prior to the inspection the surfaces were sputter coated with gold. The images were taken using a voltage of 5 kV and a working distance of approximately 10 mm.

Wettability

The sessile drop method was applied to measure the static contact angle of the pre-treated surfaces. For this purpose, a Krüss DSA 100 equipment (Germany) was employed. The measurements were performed using water droplet with a volume of 10 μL on the pre-treated composite surfaces. The contact angle was measured from each area after approximately 30 s to stabilize the water droplet. A high-resolution camera was used to capture the profile of the liquid droplet on the solid substrate. Three different areas were investigated. The average of the measured values of the three areas was considered as the average contact angle for each surface pre-treatment.

Surface Chemical Modification

X-ray Photoelectron Spectroscopy (XPS) technique was employed for identification of functional groups generated on the surface of CF-PPS composite and PPS film after plasma activation. The analyses were performed using a Kratos DLD Ultra Spectrometer operated at 225 W under ultrahigh vacuum using a monochromatic Al-Kα X-ray as the excitation source. Data processing was performed with CasaXPS software.

3.3.3. Joining Procedure

Single overlap joints were produced using displacement-controlled FSp joining equipment (RPS 100 - Harms&Wende, Germany). The overlap configuration of the joint is shown in Figure 3. The overlap area was 25.4 x 25.4 mm^2, with the PPS film placed in between the aluminum and the composite.

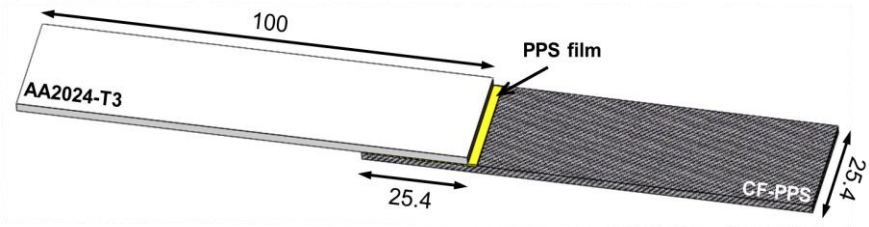

Figure 3: Configuration and dimensions (in mm) of the joining parts.

The joining parameters were selected based on our previous investigation with the same materials [14]. The selected joining parameters were: rotational speed of 1900 rpm, plunge depth of 0.8 mm, joining time of 4 s and joining pressure of 0.2 MPa. Such parameters combination provided the highest static lap-shear strength. The joints were intentionally exposed to an extensive consolidation time of 120 s after the joining process to minimize differential shrinkage of the joints due to polymer reconsolidation. The present study relies on research purposes, therefore the optimization of the consolidation time for industrial production was out of the scope of this work.

3.3.4. Mechanical Testing

The quasi-static mechanical performance of the joints was evaluated through lap shear testing under tensile loading in accordance to the ASTM D3163-01. Tests were performed using a universal testing machine Zwick/Roell 1478, with a cross-head speed of 1.27 mm min^{-1} at room temperature. The dimensions of the specimens were 100 x 25.4 mm with 25.4 x 25.4 mm^2 of overlap area, as depicted in Figure 3. Three replicates for each surface pre-treatment were tested. The average of the three tests was reported as the ultimate lap shear force (ULSF) of the joints.

4. Results and Discussion

4.1. Surface Features

The surface modifications induced by the pre-treatments applied on the parts were analyzed by roughness and contact angle measurements. Additionally, the sandblasted surfaces, which were post-activated with plasma, were investigated using XPS. Table 6 and Table 7, as well as Figures 4 to 7, summarize the results related to the mechanical surface pre-treatments.

Table 6: Average surface roughness and water contact angle on the aluminum in the as-received condition and after sandblasting.

Material	Surface Pre-treatment	Symbol	Roughness (R_a) [µm]	Contact angle [°]
Aluminum	As received	AR	0.4 ± 0.1	77 ± 2
	Sandblasting	S1	5.5 ± 0.3	19 ± 2

Table 7: Average surface roughness and water contact angle on the composite in the as-received condition and after the applied pre-treatments.

Material	Surface Pre-treatment	Symbol	Roughness (R_a) [µm]	Contact Angle [°]
Composite	As received	AR	0.4 ± 0.1	69 ± 2
	Sandblasting	S2	3.8 ± 0.2	95 ± 3
		S3	4.3 ± 0.4	98 ± 1
		S4	5.3 ± 0.6	106 ± 4
	Mechanical Grinding	M1	0.6 ± 0.1	75 ± 1
		M2	1.2 ± 0.1	88 ± 2
	Plasma Activation	S4 + P1	5.3 ± 0.6*	8 ± 2
		S4 + P2	5.3 ± 0.6*	11 ± 2

*Measured before plasma activation

The topographical view of the mechanically pre-treated surfaces (both aluminum and composite) is illustrated in Figure 4. The sandblasted specimens (S1 to S4) exhibit a modified surface with hills and valleys, whereas the mechanically ground specimens (M1 and M2) show crevices in form of uneven grooves on the surface. As can be seen in Table 7, sandblasting was the most effective surface pre-treatment in increasing the composite's surface roughness. The surface roughness of the composite was increased from 0.4 ± 0.1 µm (AR) up to 5.3 ± 0.6 µm (S4) when an incidence-blasting angle of 45^o degrees as used.

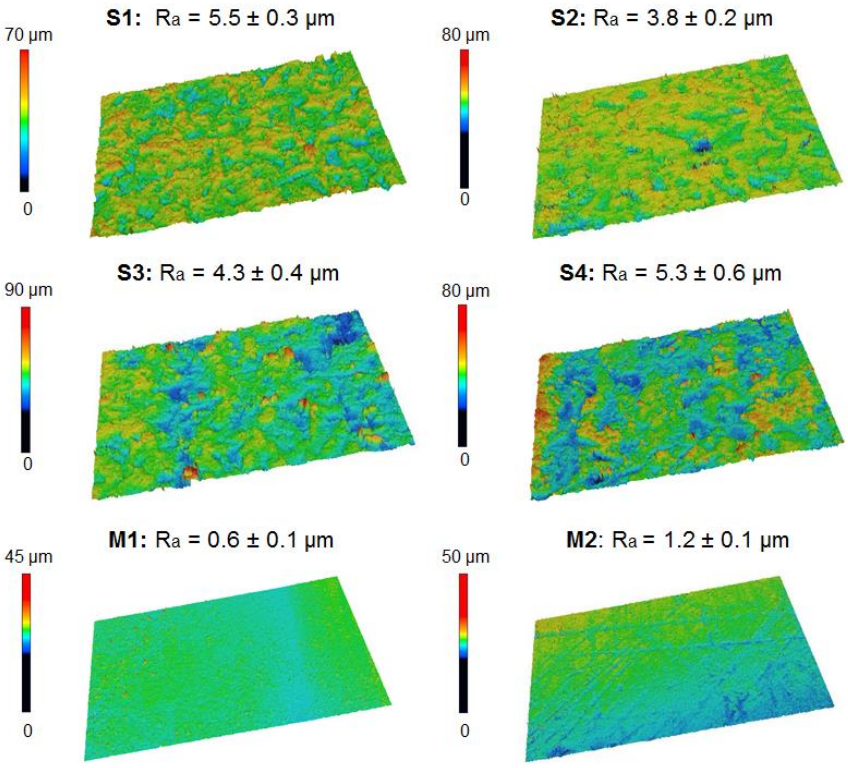

Figure 4: Topographical view and the arithmetic average roughness (R_a) of the aluminum and composite surfaces after mechanical pre-treatments, prior to the joining process. Refer to Table 5 for details of surface pre-treatments.

The sandblasting condition S4 (on the composite) removed most of the PPS matrix on the composite's surface, and the treated surface showed exposed carbon fibers as can be seen in Figure 5-A (see white arrows). During FSpJ, the molten interlayer embeds the exposed fibers, improving the micro-mechanical anchoring between the parts described in Figure 2-B. In addition, a few damaged carbon fibers appear on the surface of the composite as a result of the sandblasting (Figure 5-B).

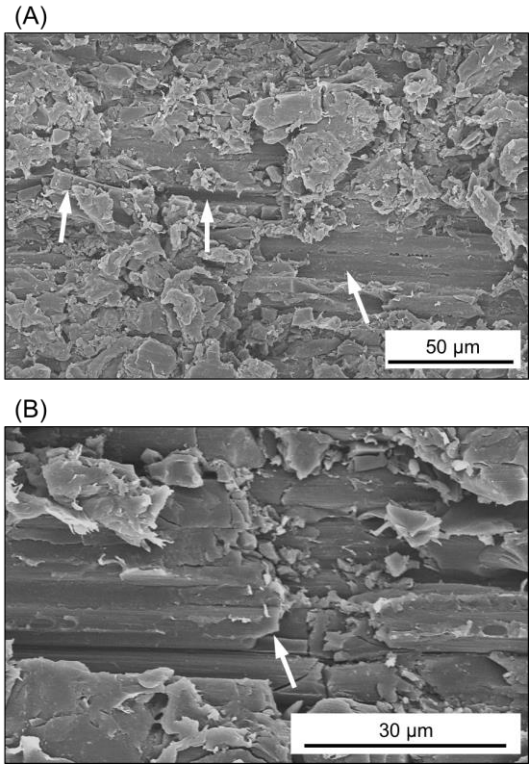

Figure 5: SEM images showing (A) the topography of sandblasted CF-PPS composite showing the partial removal of the PPS matrix and some exposed carbon fibers and (B) the sandblasted composite surface, where the arrow indicates damaged fibers.

The wettability of the surfaces was monitored using contact angle measurements. For the aluminum part, the contact angle decreased enormously by increasing the surface roughness as seen in Table 6 and illustrated in Figure 6. The increase of the effective surface area and the removal of surface contaminations are known to increase the surface energy of the metal, reducing the water contact angle [32]. Therefore, an improved wettability on the aluminum surface was achieved through sandblasting. The molten polymer can flow into the crevices on the aluminum surface during the joining process. This causes micro-mechanical interlocking between the parts, leading to an increased mechanical performance as it will be discussed in Section 4.2.

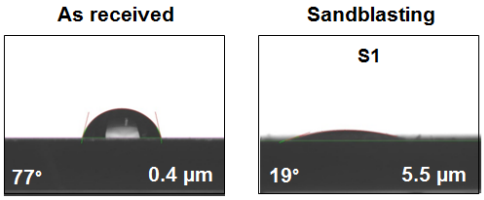

Figure 6: Representative example of water contact angle measurements, along with the average surface roughness (R_a), comparing as received and sandblasted aluminum surfaces.

A different trend was identified for the composite surface. For the mechanically-treated surfaces, the higher the surface roughness, the larger the contact angle is, as shown in Figure 7. PPS reveals a hydrophobic surface due to the rupture of chemical bindings as a result of the sandblasting abrasion [33]. Such hydrophobic forces on the polymeric surface seem to prevent the water droplet from penetrating into the irregularities of the rough PPS surface. Thus, the partial wetting of the hydrophobic surface reflects an apparent larger contact angle than the real one. Nisbet *et al.* [34] also observed increased water contact angle due to the hydrophobic character of electrospun membranes in their study. Therefore, future contact angle measurements using molten PPS should be performed to investigate the wetting behavior of the sandblasted surfaces. However, such investigation is out of the scope of this work.

In the case of the combination of sandblasting and plasma activation (S4+P1 and S4+P2) the water contact angle on the surface of the composite drastically decreased as shown in Figure 7. This decrease in the contact angle indicates the introduction of chemical groups on the surface that neutralizes the hydrophobic nature of the pre-sandblasted surface. To better understand the combined effects of the selected surface pre-treatments, XPS analysis was performed on the treated specimens. Figure 8 shows the high-resolution XPS spectra from oxygen bonds O1s region obtained from the sandblasted surface, as well as sandblasted followed by the plasma post-activation (using oxygen gas).

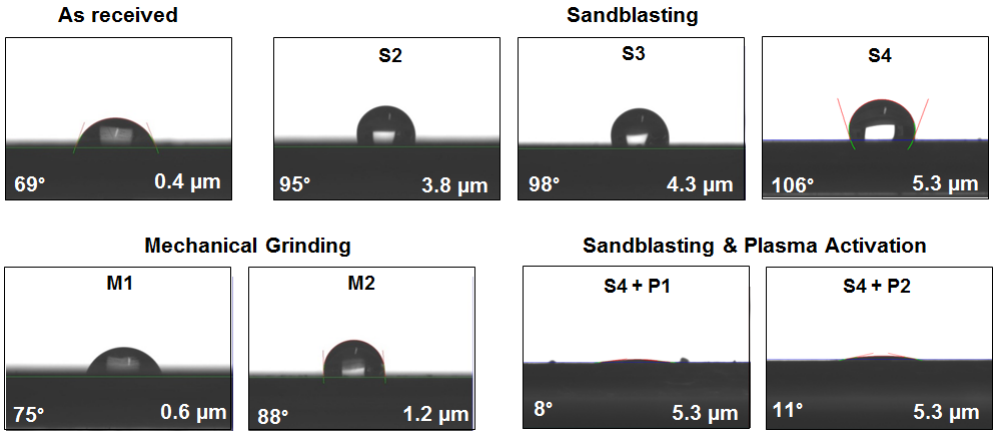

Figure 7: Representative example of contact angle measurements, along with the average surface roughness (R_a), comparing as received condition and different surface pre-treatments on the composite part.

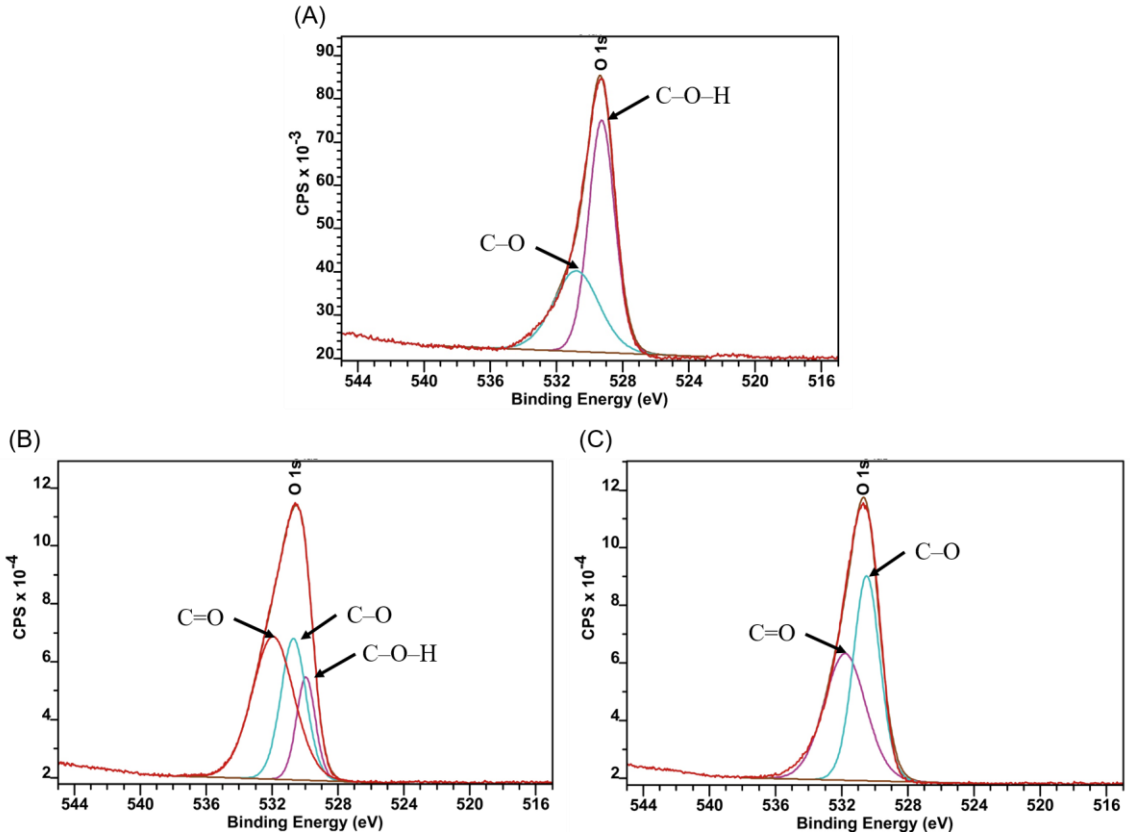

Figure 8: High-resolution XPS spectra from O1s region on the CF-PPS surface after (A) sandblasting (S4), (B) S4 + P1 (5 min), and (C) S4 + P2 (10 min).

From deconvolution of the O1s peak, three chemical groups were identified on the surfaces: C–O–H (529.7 eV), C–O (531.1 eV) and C=O (532.0 eV) [35]. The C–O–H and C–O groups may be related

to water and oxygen absorption from the atmosphere, respectively [36,37]. One can observe that the intensity of C–O groups progressively increased as the sandblasted specimens were plasma-treated for 5 and 10 minutes (Figure 8). In contrast, the C–O–H groups were progressively eliminated from the surfaces as the plasma activation was applied (Figure 8). It suggests that the plasma-treated surfaces absorbed oxygen ions, creating C–O groups whereas eliminating impurities (C–O–H group). Nevertheless, the C=O group was identified only for the plasma-treated specimens as a result of the induced bonds during treatment (Figure 8-B and C).

In the whole spectra, the intensity of oxygen significantly increased from 85 $x10^3$ CPS (for sandblasting) to 11.5 $x10^4$ CPS and 11.8 $x10^4$ CPS for the post-activated surfaces S4 + P1 and S4 + P2, respectively (see graphs in Figure 8). These results suggest that the surface free energy of the PPS was increased due to the induced bonds with oxygen, because of the plasma post-treatment. Therefore, the increase in surface energy resulted in improved wettability of the composite surface in comparison to the sandblasted specimens (Figure 7). This is in agreement with the increase in wettability of PPS plasma-activated in adhesively bonded joints observed by Anagreh *et al.* [38]. In this work, contact angle measurements also demonstrated that the surface energy of the PPS increased with the time of plasma treatment [38].

4.2. Quasi-Static Mechanical Performance

Figure 9 presents the ultimate lap shear force (ULSF) of friction spot joints with film interlayer produced with different composite surface pre-treatments, as well as its correlation with surface roughness.

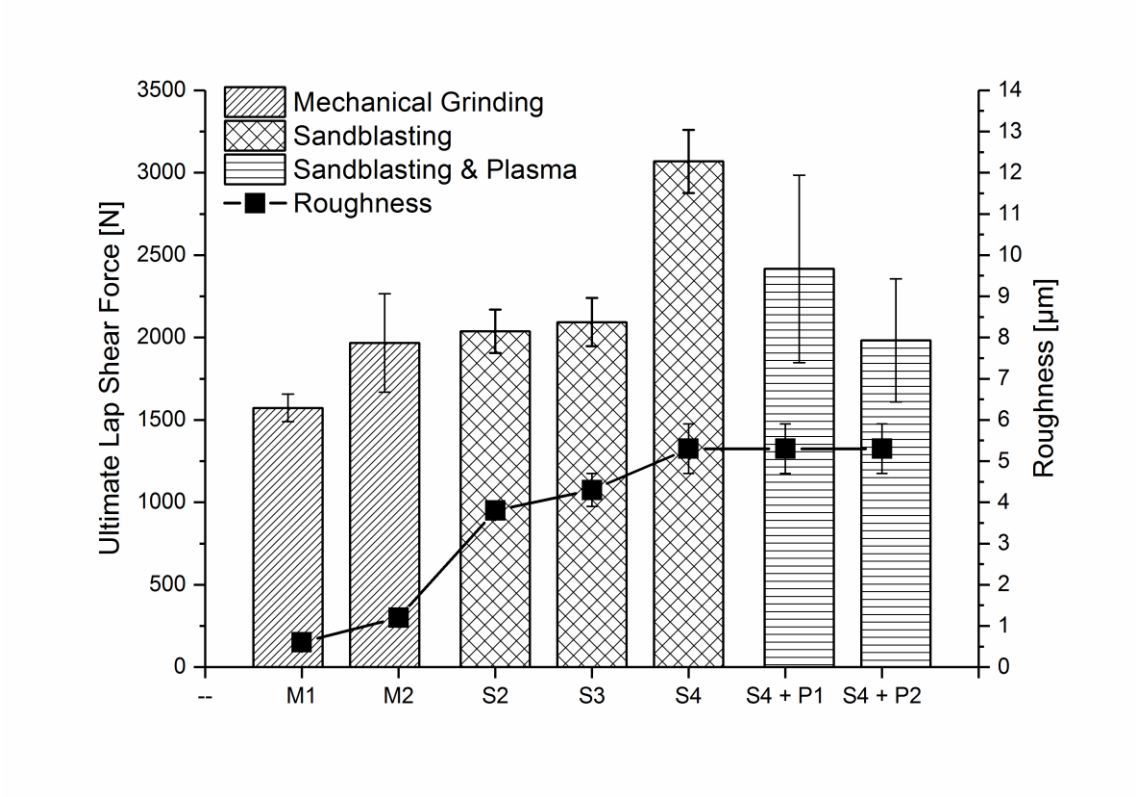

Figure 9: Ultimate lap shear force of FSp joints produced with different composite surface pre-treatments and the respective surface roughness.

One can observe from Figure 9 that an increase in surface roughness directly increases the lap shear strength of the joint. The composite surface with the highest roughness (S4: R_a = 5.3 ± 0.6 µm, Table 7) led to a joint approximately 95% stronger (S4: ULSF = 3068 ± 192 N) than the joint with the smallest roughness (M1: R_a = 0.6 ± 0.1 µm, Table 7; ULSF = 1573 ± 84 N). The increase in roughness creates crevices on the surface and enlarges the effective contact area, contributing to the micro-mechanical interlocking and establishing the adhesion forces as discussed next.

On one hand mechanical grinding resulted in lower average surface roughness. Besides the lower surface roughness, the crevices are distributed in the form of uneven grooves on the surface, as previously showed in Figure 4. On the other hand, sandblasting produced higher average surface roughness. In this case, additionally to the higher surface roughness achieved, the crevices are well distributed in the shape of hills and valleys on the surface (Figure 4). The combination of shape and distribution of the crevices leads to a larger amount of effective sites for mechanical interlocking in the sandblasted specimens. In

this case, a better micro-mechanical interlocking between the composite and the PPS film is achieved, leading to stronger joints.

Additionally, the increase in roughness enlarges the effective contact area. As it was previously discussed [39], intermolecular diffusion may take place between PPS interlayer and PPS matrix at the joint's interface. Considering the diffusion phenomenon, a larger contact area may increase the possibility of intermolecular migration between composite's PPS matrix and PPS film. Therefore, the higher surface roughness achieved with sandblasting (S4) may also contribute to the establishment of adhesion forces between the joining parts through the increase in contact area, strengthening the joint.

The plasma activation, on the other hand, did not contribute to the mechanical strength of the friction spot joints (Figure 9) in this work. The sandblasted joints showed an ULSF of up to 3068 ± 192 N. After the plasma activation (S4 + P1 and S4 + P2) a decrease of 21% (2416 ± 568 N) was observed for S4 + P1 (5 min activation) and 35% (1983 ± 373 N) for S4 + P2 (10 min activation). There are two hypotheses to explain this phenomenon. Although functional groups were identified on the composite surface prior to the joining process, due to the melting of PPS matrix in the center of the joint during the FSpJ process, it is believed that the plasma activation was eliminated. Another plausible argument for the losses in mechanical performance for plasma-treated specimens can be associated with the plasma activation process itself. During the plasma treatment, temperatures up to 110°C were achieved due to the power of plasma generation. Therefore, the exposition of the sandblasted composite to these temperatures may have led to the local softening of the PPS matrix. As a result, closure of some crevices on the sandblasted surface may have occurred, decreasing the effective contact area between the parts. This leads to a decreased micro-mechanical interlocking between the PPS matrix and interlayer. Hence, a reduction in joint lap shear strength was observed. The decrease in ultimate lap shear force was pronounced for S4 + P2 because of the longer time of plasma treatment. Further investigations should be carried out to prove these two hypotheses.

The fracture surface of the joints was also visually evaluated, as it can be seen in Figure 10.

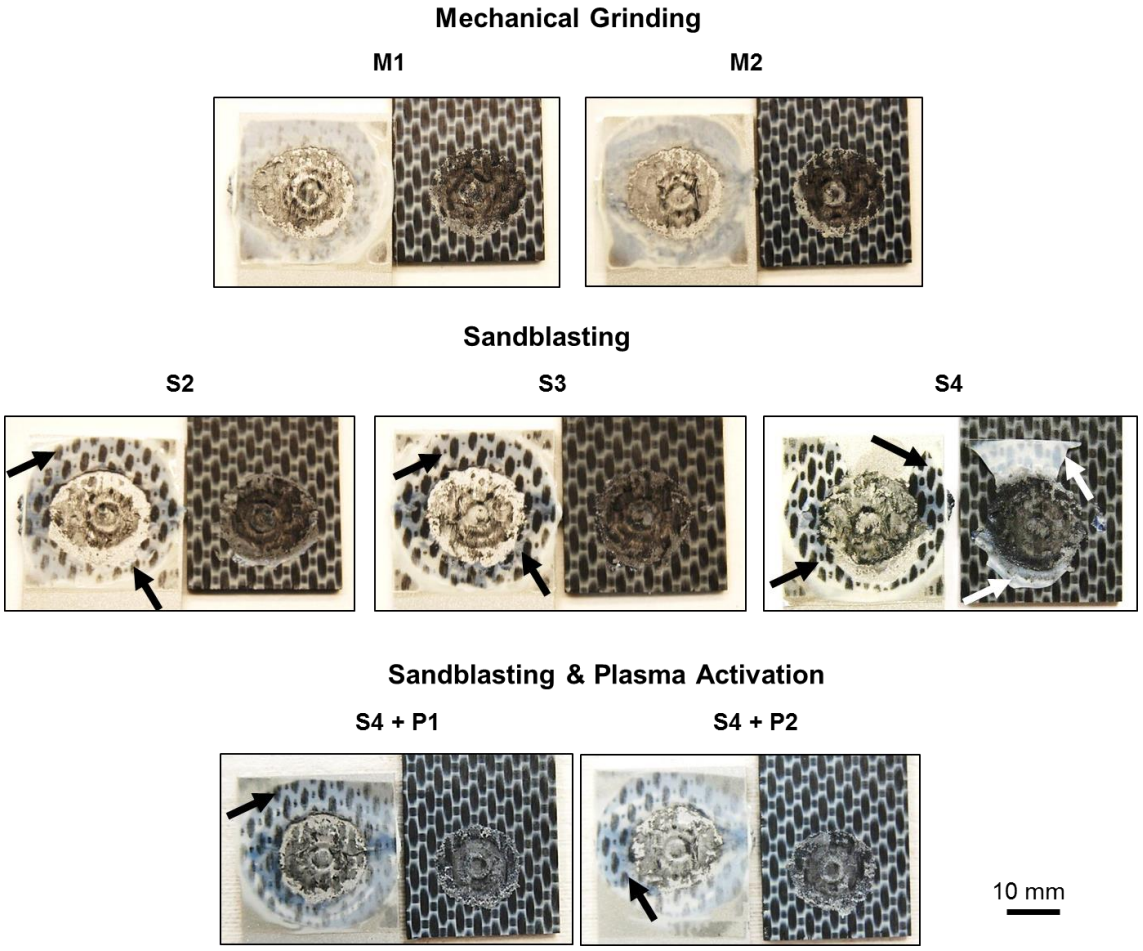

Figure 10: Representative examples of the fracture surface of FSp joints produced with different composite surface treatments.

One observes that, regardless of the type of composite's pre-treatment, the interlayer remains mostly attached to the surface of the aluminum (Figure 10) after lap shear testing. This is mainly due to the higher temperatures achieved on the aluminum surface during the joining process [14]. It favors melting, hence the decrease in viscosity of the PPS film in contact with the surface of the aluminum. Thus, the rough aluminum's surface after sandblasting (S1 treatment, see Table 5) is more effectively wet by the molten PPS interlayer during the joining process than the composite surface. Additionally, the wetting of the aluminum surface was improved after sandblasting, as suggested by the contact angle measurement (Figure 6). In this way, the irregularities on the aluminum surface are filled with the molten PPS leading to effective micro-mechanical anchoring between the aluminum and PPS interlayer.

Considering the different composite surface pre-treatments, a pronounced difference can be observed from the fracture surfaces in Figure 10. An impression of the composite was identified on the surface of the interlayer in the case of the specimens sandblasted. The impressions are presented in the form of black spots resembling the weave pattern of fiber reinforcement, as indicated by black arrows in S2, S3 and S4 specimens (Figure 10). However, this was not the case for the mechanically ground specimens (Figure 10). Detailed evaluation of these impressions by SEM analysis was presented and explained in [14]. Briefly, the impressions contain pieces of carbon fibers removed from the PPS matrix, which remained attached to the interlayer. This is an indication of an effective micro-mechanical interlocking at the interface of interlayer-composite achieved with the sandblasted specimens.

In addition, it is possible to identify a part of the consolidated interlayer on the composite part of the specimens sandblasted by the S4 procedure (white arrows in Figure 10 – S4). This suggests that the strength of the interlayer-composite interface is comparable to the metal-interlayer interface in this case. The S4 pre-treatment generated the highest roughness on the composite surface among all specimens, consequently led to the highest mechanical strength of the joints (3068 ± 192 N).

The fracture surface of S4 + P1 and S4 + P2 specimens also presented the black impressions on the interlayer surface since they were subjected to sandblasting prior to the plasma activation. However, the intensity of the black spots is not as visually pronounced as the fracture surface of S4 (Figure 10). The less pronounced black impressions might be an indication of less effective micro-mechanical interlocking. As previously mentioned, the exposure to high temperature during plasma treatment might cause softening of the PPS matrix and closure of some of the crevices. It can be also observed from Figure 10 that the fracture surface of the S4 + P2 specimen visually presents even smaller amounts of black impressions compared to the S4 + P1 specimen. This is probably due to the longer plasma-treated time used for S4 + P2. As a result, joints produced with S4 + P2 presented lower average ultimate lap shear forces (1983 ± 373 N, Figure 9) than S4 + P1 specimens (2416 ± 568 N, Figure 9).

5. Conclusions

Friction spot joints of AA2024-T3 and CF-PPS were produced with additional PPS film interlayer. Mechanical grinding, sandblasting and sandblasting combined with plasma activation were performed on the composite part to enhance the interfacial adhesion between the composite and PPS film. The composite surface with the highest roughness (S4: R_a = 5.3 ± 0.6 µm) led to the joints approximately

95% stronger (S4: ULSF = 3068 ± 192 N) than the joints with the smallest roughness (M1: R_a = 0.6 ± 0.1 µm; ULSF = 1573 ± 84 N). The increase in roughness generated crevices on the surface and enlarged the effective contact surface area. This led to a better micro-mechanical interlocking between the molten PPS film and the composite surface, resulting in the higher strength as well. The plasma activation did not contribute to the mechanical strength of the FSp joints in this work. The sandblasted (S4) joint showed an average ULSF of 3068 ± 192 N. After the plasma activation (S4 + P1 and S4 + P2) a decrease of 21% (2416 ± 568 N) was observed for S4 + P1 (5 min activation) and 35% (1983 ± 373 N) for S4 + P2 (10 min activation). It is believed that the plasma activation could be lost due to the high temperatures achieved during the joining process and the resultant softening/melting of the PPS matrix at the composite surface. Moreover, during the plasma treatment, local softening of the PPS matrix may induce closure of some crevices on the sandblasted surface. Thus, the effective contact area was decreased as well as the micro-mechanical interlocking between the joining parts. Therefore, a reduction in joint lap shear strength was observed. All in all, the sandblasted specimens with the optimized parameters (S4) produced the strongest friction spot joints in this study. Impressions containing pieces of carbon fibers removed from the PPS matrix were identified on the interlayer fracture surface after lap shear testing. This is an indication of an effective micro-mechanical interlocking at the interface of interlayer-composite achieved with the sandblasted specimens.

Acknowledgments

This work was supported by Helmholtz Association, Germany (Young Investigator Group, "Advanced Polymer Metal Hybrid Structures", Grant number VH-NG-626), FAPESP - São Paulo Research Foundation, Brazil (Process 2014/09271-0) and CNPq - National Council for Scientific and Technological Development, Brazil (Process 304169/2014-5).

References

[1] Faivre V, Morteau E. Airbus Tech Mag (FAST). Damage Tolerant Composite Fuselage Sizing, Characterization of Accidental Damage Threat 2011;48:10–6.

[2] BMW i3, the inside story: what it's made of, how it's made. SAE International. (http://articles.sae.org/12056/). Accessed on June, 2016.

[3] TenCate Advanced Armour will provide ballistic solutions for the Embraer KC-390. Composites World. (http://www.compositesworld.com/news/tencate-advanced-armour-will-provide-ballistic-solutions-for-the-embraer-kc-390). Accessed on June, 2016.

[4] Messler RW. Joining of Materials and Structures: From Pragmatic Process to Enabling Technology. 1 edition. Butterworth-Heinemann; 2000.

[5] Habenicht G. Applied Adhesive Bonding: A Practical Guide for Flawless Results. 1 edition. Weinheim: Wiley-VCH; 2009.

[6] Ageorges C, Ye L. Resistance Welding of Metal/Thermoplastic Composite Joints. Journal of Thermoplastic Composite Materials 2001;14:449–75. doi:10.1106/PN74-QXKH-7XBE-XKF5.

[7] Feistauer EE, Guimarães RPM, Ebel T, dos Santos JF, Amancio-Filho ST. Ultrasonic joining: A novel direct-assembly technique for metal-composite hybrid structures. Materials Letters 2016;170:1–4. doi:10.1016/j.matlet.2016.01.137.

[8] Jung KW, Kawahito Y, Katayama S. Laser direct joining of carbon fibre reinforced plastic to stainless steel. Science and Technology of Welding and Joining 2011;16:676–80. doi:10.1179/1362171811Y.0000000060.

[9] Mitschang P, Velthuis R, Didi M. Induction Spot Welding of Metal/CFRPC Hybrid Joints. Advanced Engineering Materials 2013;15:804–13.

[10] Amancio-Filho ST, dos Santos J. European Patent 2329905B1, 2012.

[11] Amancio-Filho ST, Bueno C, dos Santos JF, Huber N, Hage Jr. E. On the feasibility of friction spot joining in magnesium/fiber-reinforced polymer composite hybrid structures. Materials Science and Engineering: A 2011;528:3841–8. doi:10.1016/j.msea.2011.01.085.

[12] Esteves JV, Goushegir SM, dos Santos JF, Canto LB, Hage Jr. E, Amancio-Filho ST. Friction spot joining of aluminum AA6181-T4 and carbon fiber-reinforced poly(phenylene sulfide): Effects of process parameters on the microstructure and mechanical strength. Materials & Design 2015;66:437–45. doi:10.1016/j.matdes.2014.06.070.

[13] Goushegir SM, dos Santos JF, Amancio-Filho ST. Friction Spot Joining of Aluminum AA2024 / Carbon-Fiber Reinforced Poly(phenylene sulfide) composite single lap joints: microstructure and mechanical performance. Materials & Design 2014;50:196–206. doi:10.1016/j.matdes.2013.08.034.

[14] André NM, Goushegir SM, dos Santos JF, Canto LB, Amancio-Filho ST. Friction Spot Joining of aluminum alloy 2024-T3 and carbon-fiber-reinforced poly(phenylene sulfide) laminate with additional PPS film interlayer: Microstructure, mechanical strength and failure mechanisms. Composites Part B: Engineering 2016;94:197–208. doi:10.1016/j.compositesb.2016.03.011.

[15] Chang B, Shi Y, Shijie D. Comparative studies on stresses in weld-bonded, spot-welded and adhesive-bonded joints. Journal of Materials Processing Technology 1999:230–6.

[16] André NM. Friction Spot Joining of aluminum alloy 2024-T3 and carbon-fiber-reinforced polyphenylene sulfide composite laminate with additional PPS film interlayer. Master thesis. Federal University of São Carlos, 2015.

[17] Baldan A. Adhesively-bonded joints in metallic alloys, polymers and composite materials: Adhesives, adhesion theories and surface pretreatment. Journal of Materials Science 2004;39:1–49.

[18] Critchlow GW, Brewis DM. Review of surface pretreatments for aluminium alloys. International of Journal Adhesion and Adhesives 1996;16:255–75.

[19] Wingfield JRJ. Treatments of Composite Surfaces for Adhesive Bonding. International Journal of Adhesion & Adhesives 1993;3:151–6.

[20] Encinas N, Pantoja M, Abenojar J, Martínez MA. Control of Wettability of Polymers by Surface Roughness Modification. Journal of Adhesion Science & Technology 2010;24:1869–83. doi:10.1163/016942410X511042.

[21] Ebnesajjad S. Chapter 5 - Theories of Adhesion. In: Ebnesajjad S, editor. Surface Treatment of Materials for Adhesive Bonding (Second Edition), Oxford: William Andrew Publishing; 2014, p. 77–91.

[22] Medical Device & Diagnostic Industry (MDDI). Surface Modification Using Low-Pressure Plasma Technology, 2000. < http://www.mddionline.com/article/surface-modification-using-low-pressure-plasma-technology>. Accessed on June, 2016.

[23] Kim JK, Lee DG. Investigation of optimal surface treatments for carbon/epoxy composite adhesive joints. Journal of Adhesion Science and Technology 2003;3:329–52.

[24] Iqbal HMS, Bhowmik S, Benedictus R. Surface Modification Of High Performance Polymers by Atmospheric Pressure Plasma and Failure Mechanism of Adhesive Bonded Joints. International Journal of Adhesion & Adhesives 2010:418–24.

[25] Esteves JV, Amancio-Filho S, dos Santos J, Canto LB, Hage Jr E. Friction Spot Joining of aluminum 6181-T4 and carbon fiber reinforced poly(phenylene sulfide). In: ANTEC - Society of Plastics Engineers, Orlando, FL, USA, 2012.

[26] “Henry Granjon” prize for the PhD thesis "Friction Spot Joining of Metal-Composite Hybrid Structures" of Seyed M. Goushegir, Category A, International Institute of Welding, Melbourne, 2016.

[27] “Rising Star", Category: Joining Techniques, Automotive Circle International, Nürnberg, Germany, 2015.

[28] Goushegir SM. Friction Spot Joining of Metal-Composite Hybrid Structures. PhD thesis. Technical University of Hamburg, Germany, 2015.

[29] Technical datasheet of aluminium alloy 2024-T3. Constellium France, 2012.

[30] Technical datasheet of CETEX® PPS. Tencate Advanced Composites, 2009.

[31] Technical datasheet of PPS film. LITE P, 2009

[32] Abdallah W, Buckley J, Carnegie A, Edwards J, Herold B, Fordham E. Fundamentals of Wettability. Oilfield Review, Bahrain: 2007, p. 46–61.

[33] Dropwise steam condensation on various hydrophobic surfaces: Polyphenylene sulfide (PPS), polytetrafluoroethylene (PTFE), and self-assembled micro/nano silver (SAMS). International Journal of Heat and Mass Transfer 2015;89:353-358.

[34] Nisbet DR, Rodda AE, Finkelstein DI, Horne MK. Surface and Bulk Characterisation of Electrospun Membranes: Problems and Improvements. Colloids and Surfaces B: Biointerfaces 2009;71:1–12.

[35] N. N, NIST X-ray Photoelectron Spectroscopy Database, Version 4.1, National Institute of Standards and Technology, Gaithersburg, 2012.

[36] Petti D, Cantoni M, Leone M, Bertacco R, Rizzi E. Activation of Zr–Co–rare earth getter films: An XPS study. Applied Surface Science 2010;256:6291–6. doi:10.1016/j.apsusc.2010.04.006.

[37] Sánchez-Amaya JM, Blanco G, Garcia-Garcia FJ, Bethencourt M, Botana FJ. XPS and AES analyses of cerium conversion coatings generated on AA5083 by thermal activation. Surface and Coatings Technology 2012;213:105–16. doi:10.1016/j.surfcoat.2012.10.027.

[38] Anagreh N, Dorn L, Bilke-Krause C. Low-Pressure Plasma Pretreatment of Polyphenylene Sulfide (PPS) Surfaces for Adhesive Bonding. International Journal of Adhesion & Adhesives 2007:16–22.

[39] André NM, Goushegir SM, Dos Santos JF, Amancio-Filho ST, Canto LB. Influência da Espessura do Filme Polimérico Intermediário na Resistência Mecânica de Juntas Híbridas de Alumínio 2024-T3 e CF-PPS Produzidas por União Pontual por Fricção. In: National Congress of Welding (CONSOLDA), Salvador, Brazil, 2015.